Physics of Fluids

Transient, nonaxisymmetric modes in the instability of unsteady circular Couette flow. Laboratory and numerical experiments

Cite as: Physics of Fluids **7**, 324 (1995); https://doi.org/10.1063/1.868630
Submitted: 27 April 1993 . Accepted: 12 October 1994 . Published Online: 02 September 1998

G. P. Neitzel, C. S. Kirkconnell, and L. J. Little

View Online

Export Citation

ARTICLES YOU MAY BE INTERESTED IN

Mechanism of elastic instability in Couette flow of polymer solutions: Experiment
Physics of Fluids **10**, 2451 (1998); https://doi.org/10.1063/1.869764

AIP Publishing

© 1995 American Institute of Physics.

Transient, nonaxisymmetric modes in the instability of unsteady circular Couette flow. Laboratory and numerical experiments

G. P. Neitzel and C. S. Kirkconnell
The George W. Woodruff School of Mechanical Engineering, Georgia Institute of Technology, Atlanta, Georgia 30332-0405

L. J. Little
Department of Mechanical and Aerospace Engineering, Arizona State University, Tempe, Arizona 85287-6106

(Received 27 April 1993; accepted 12 October 1994)

Laboratory and numerical experiments were conducted to quantitatively determine the modal structure of transient, nonaxisymmetric modes observed during the instability of an impulsively initiated circular-Couette flow. The instability develops initially as an axisymmetric, Görtler-vortex state and persists ultimately as a steady, axisymmetric Taylor-vortex state of different wavelength. The transition between these two states results from the instability of the Görtler mode combined with the underlying developing swirl flow and is dominated by nonaxisymmetric modes. The laboratory experiments employed flow visualization coupled with digital video and image-processing techniques; numerical experiments were performed using the spectral-element code, NEKTON. © *1995 American Institute of Physics.*

I. INTRODUCTION

Circular Couette flow (CCF) has served as an effective test bed for studying complex transitions to chaos, the influence of finite geometry on pattern-selection mechanisms and the effects of time-dependent basic states. The stability properties of time-dependent circular-Couette flow have been of interest for some time, serving as a model for eventual studies of unsteady effects in more complicated situations. Unsteady CCF offers the luxuries of a simple geometry, amenable to both analyses and experiment, and a transition sequence which can be as simple or complex as desired through the adjustment of the geometrical and dynamical parameters involved.

The flow of interest in the present case is one which combines elements of pattern selection not with finite geometry, but with a time-varying basic state. Consider a pair of concentric circular cylinders shown in Fig. 1 of radii a and $b>a$ which enclose a viscous, incompressible fluid of kinematic viscosity ν; the overall length of the system is L. Prior to some initial time, the entire system is assumed to be in a state of rigid-body rotation with angular speed Ω about the symmetry axis. At time $t=0$, the outer cylinder is impulsively brought to rest, giving rise to an unsteady basic state which develops from the outer wall of the annulus. This basic state is subject, after an initial period of guaranteed stability,[1] to centrifugal instability. The flow is characterized by two dimensionless geometric parameters, the *radius ratio* $\eta=a/b$ and the *aspect ratio* $\Gamma=L/d$, where $d=b-a$ is the gap width, and a single dimensionless dynamic parameter, which we choose to be the *Reynolds number* $\mathrm{Re}=\Omega d^2/\nu$.

The flow just described has been studied previously. Chen and Neitzel[1] and Neitzel[2] used energy-stability theory to determine sufficient conditions for stability while Kohuth and Neitzel[3] conducted flow-visualization laboratory experiments to determine the onset time and structure of the *initial* instability. These experiments, performed with a wide-gap ($\eta=0.5$) apparatus, uncovered, at the higher Reynolds numbers considered, an interesting sequence of events which motivated the present work. The *initial* appearance of instability to the nearly pure-swirl basic state is in the form of *axisymmetric*, counter-rotating vortices which form once the layer near the outer cylinder has thickened to the point where the centrifugal forces can dominate the viscous forces. The axisymmetric nature of the initial instability is in agreement with energy-stability calculations.[1] However, since the underlying basic state continues to develop, the length scale associated with the potentially unstable region changes. Indeed, after a large time has passed, the basic-state swirl flow is subject to centrifugal instability across the entire gap and it is then the larger gap width which characterizes the scale of the finally appearing structure. For this flow at the radius ratio and Reynolds numbers of interest, the final flow is in the form of *axisymmetric* Taylor vortices which are roughly square in cross section. Consequently, the initial, smaller-scale vortices must give way to a larger-scale Taylor-vortex state. The adjustment between these two axisymmetric states was observed to occur *nonaxisymmetrically* in the Kohuth and Neitzel experiments. It is the characterization of the azimuthal structure of this transition, at least at its onset, which is the goal of the present research.

We shall refer to the vortices observed as a result of the initial instability as Görtler vortices, since they result from a centrifugal instability and their size is related to the thickness of the potentially unstable layer near the outer, concave wall. Although, at any instant of time, this layer thickness is independent of the azimuthal (streamwise) coordinate, the thickness increases with time analogous to the spatial changes observed in the usual Görtler situation.[4] Therefore, from a Lagrangian viewpoint, fluid particles are moving into a region of increasing boundary-layer thickness much as in the boundary layer on a concave plate. The scale of the Görtler vortices observed in the present situation is dictated by the thickness of this layer at the onset time of the initial insta-

 1070-6631/95/7(2)/324/11/$6.00 © 1995 American Institute of Physics

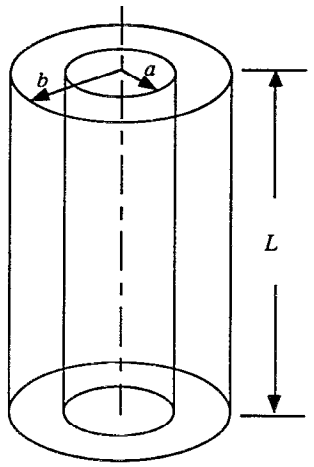

FIG. 1. Taylor–Couette geometry.

bility. At the Reynolds numbers of interest, the presence of the inner cylinder does not appear to affect this onset time, as evidenced by the agreement between the onset times for Couette flow measured by Kohuth and Neitzel[3] and those for spin-down to rest determined by Mathis and Neitzel.[5] The vortices that are first apparent during the instability of spin-down also become unstable; the transition is less complicated in the present case, however, due to the presence of the inner cylinder and the ultimate establishment of a Taylor-vortex state. Also, the finite length of the apparatus does not appear to be a factor in determining the scales associated with the early transitions since the results of spin-down experiments in cylinders of widely varying aspect ratio are identical.[5] Consequently, this model problem appears to be a good candidate for investigating the influence of a time-dependent basic state on pattern selection.

The influence of a time-developing basic state on pattern selection may be important in some practical situations. With regard to CCF, Coles[6] demonstrated the existence of multiple states at fixed control-parameter values, these being achieved by altering the way in which the final state was approached. More recently, Benjamin and Mullin[7] investigated such multiple states, including so-called "anomalous modes" (rotating in the "wrong" direction adjacent to end walls), also achieved through time-dependent manipulation of the boundary conditions. Uniformly accelerated CCF has received a reasonable amount of attention. Worthy of note in the present context are the experiments of Burkhalter and Koschmieder,[8] which were concerned with the influence of the sudden start of the inner cylinder on steady, axisymmetric Taylor-vortex patterns. Subsequent attempts to compute this flow[9] using an axisymmetric computational model met with difficulty at the highest Reynolds number attempted, and one reason for this difficulty was speculated to be the presence of transient, non-axisymmetric modes in the laboratory experiments.

As mentioned above, the focus of the earlier laboratory experiments[3] was the determination of the onset time and axial vortex wavelength of the initial, axisymmetric Görtler instability. An early effort by Myers[10] to quantify the structure of the nonaxisymmetric transition employed a low-resolution, two-dimensional photodiode array, but suffered from inadequate spatial resolution to permit a reliable determination of the azimuthal spectra during the transition. The present laboratory experiments utilize more sophisticated digital video data acquisition.

The numerical solution of the unsteady, three-dimensional (3-D) Navier–Stokes equations is a task which may be undertaken, given recent advances in computer hardware and software. However, while steady 3-D flows have been computed for very complex geometries (particularly for compressible cases), there is not a large body of numerical work for unsteady, 3-D incompressible flow; what there is restricted to relatively simple geometries. Once again, CCF is an attractive candidate for the reasons previously stated. Such computations for wavy-vortex flow have been performed by Moser, Moin, and Leonard,[11] Marcus,[12] and Coughlin and Marcus.[13] This problem differs from those just cited, however, in that the sequence of instabilities observed leads to a flow with a variety of length scales, not all of which can be represented in the computation. For the numerical experiments of this paper, the problem of interest is solved numerically using a commercially available, spectral-finite-element code called NEKTON. Numerical solutions were attempted for one of the cases considered experimentally; laboratory and numerical results will be compared for this case.

II. LABORATORY EXPERIMENTS

A. Apparatus, instrumentation, and procedure

The physical Taylor–Couette apparatus existed from previous experiments conducted by Kohuth and Neitzel[3] and Myers;[10] details of the design and of the brake/clutch mechanism used to effect the nearly impulsive stop may be found in the paper by Kohuth and Neitzel. The flow regime has an aspect ratio of $\Gamma=37$ and a radius ratio of $\eta=0.5$. The end walls of the apparatus rotate with the outer cylinder, so that, following the initiation of the experiment, they are fixed. Spin-down experiments by Mathis and Neitzel[5] determined the onset of instability to be due primarily to the spontaneous nucleation of disturbances rather than to the propagation of an end-wall vortex front and this conclusion is presumed to be valid for the present experiments.

The fluid used for these experiments is Dow Corning 200 silicone oil with a nominal viscosity of ten centistokes at 25 °C. Flow visualization is accomplished by seeding the silicone oil with grade 602 aluminum flakes from Alcoa Albron with a nominal size of 3 μm×7 μm×2 μm. An empirical relationship between the temperature of the fluid and the kinematic viscosity was derived from measurements made on the silicone–oil/aluminum-flake mixture. The flakes have a tendency to align themselves with the shear of the flow,[14] visually revealing the flow structure. Since the density of the aluminum flakes is slightly greater than that of silicone oil, they settle to the bottom of the apparatus over a period of time, requiring the fluid to be mixed before each experiment. The flow was seeded with just enough material so that the inner cylinder was not visible and the internal flow structure was masked during an experimental run. The result was that

flow patterns were observed only at the inner surface of the outer cylinder.

Previous investigations[3,10] of this flow have used either one-dimensional (1-D) or two-dimensional (2-D) photodiode arrays coupled with flow visualization to attempt to quantify its structure. While these methods were successful in identifying the axial wavelength of the initially appearing axisymmetric vortex structure,[3] the use of a low-resolution 2-D array was unsuccessful in characterizing the azimuthal structure during the nonaxisymmetric transition from Görtler–Taylor-vortex flow.[10]

The present work utilizes a video imaging/digitizing system. The primary components are an Imaging Technology, Inc. (ITI) variable-scan frame-grabber (VFG) printed circuit board and a Dage-MTI, Inc. CCD-72 solid-state camera. Peripheral components of the system are a Sony Trinitron color video monitor and a Mitsubishi BV-1000 super-VHS video cassette recorder. Finally, an ITEX-VFG subroutine library and an image analysis software package from Bioscan were used to facilitate the data acquisition, reduction, and interpretation tasks.

The ITI VFG has the capability to accept either a standard RS-170 interlaced signal (30 frames per second) or a noninterlaced signal from a fast-frame-rate camera. Preliminary tests determined that there was no detectable degradation of image quality due to the 1/60 s lag between the capture of the even and odd fields in the interlaced mode. Therefore, for ease of calibration and timing, data acquisition was performed in the interlaced mode.

The remainder of the system was designed around the capabilities of the VFG board. With the Mitsubishi super-VHS recorder, stable images are obtainable in both slow motion and frame-by-frame modes, thus allowing the flow to be visually examined effectively and accurately at known instants in time. Since each experiment was recorded on video tape simultaneously with the digital data acquisition, a visual record was available for comparison with onset times and wavelengths determined from the analysis of the digital data. Though not necessary for these experiments, the data from the video tape can be post-processed and digitized, if desired, by selecting the VCR as the input source for the VFG.

While the azimuthal flow structure is of primary interest, it is also desirable to obtain quantitative information on the axial structure. Since the initial instability is axisymmetric, its onset time can be determined by inspection of the time history of an axially sampled flow pattern. Digitizing the entire field of view would have reduced the data-acquisition rate intolerably compared to the speed at which changes take place in the flow. Instead, two orthogonal lines of pixels were digitized to provide the desired data. The horizontal line (480 pixels) was defined by the center row of pixels to minimize the manipulation required to correct for curvature, and the vertical line (380 pixels) corresponded with the centerline of the cylinders. Due to the finite computational time required to write the data to the PC's ram drive, the data-acquisition rate was limited to ten frames per second.

Prior to the initiation of each experiment, the silcone oil was vigorously mixed to ensure even distribution of the aluminum flakes, the lighting optimized to reduce glare and the camera image calibrated, and finally, the temperature of the liquid was measured to allow the determination of its viscosity. The experiments themselves are carried out under the control of the PC, which establishes the initial state, initiates the unsteady flow, and coordinates the data acquisition. The control/data-acquisition program prompts the user for the desired Reynolds number, measured temperature of the fluid, optical calibration factors, and the pixel column number corresponding to the centerline of the cylinders. The computer uses the fluid temperature to calculate the viscosity, and hence, knowing the desired Reynolds number, the required angular speed, then initiates a ramping routine which is exited once this speed is bracketed. A bisectioning routine is then executed until the difference between the desired speed and the actual speed is within a specified tolerance. The speed is held constant for 1.5 gap-diffusion times (d^2/ν) to ensure rigid-body rotation. The final task for the control system is the initiation of the unsteady flow, which is accomplished by sending signals which sequentially disengage the clutch and engage the brake.

B. Data reduction and laboratory results

Figure 2 shows a sequence of photographs from one of the experiments at Re=300 which identifies the different flow regimes. Table I provides a summary of onset time and spatial data for the five Reynolds numbers examined.

The onset times and wavelengths of interest were determined by analyzing the video-taped record of the experiments along with power spectra determined from discrete Fourier transforms (DFTs) of the luminance data. Before the DFTs could be calculated, however, steps had to be taken to condition the raw data. Slight variations in illumination were never totally eliminated since the aluminum flakes have a tendency to stick to the outer cylinder, and the outer cylinder itself is not perfectly uniform. To eliminate contamination of the data by these factors, the luminance data from the first frame of data taken following the impulsive stop were subtracted from all subsequent frames. Noise introduced by glare from individual aluminum flakes was reduced by smoothing (using a five-point running average) the data before calculating the power spectra.

Once power spectra were calculated, the results were displayed in two formats to determine the quantities of interest: (i) the time history of amplitude for selected wave numbers and (ii) the time history of the *sum* of the amplitudes of all of non-DC spectral components. Either of the graphs may be employed to determine the onset time of interest, but the second type proved more reliable when compared with a visual examination of the video tapes. Figure 3 shows the time history of the *sum* of all significant non-DC components for the axial direction for a typical case. The quantity k referred to in the caption of this figure (and again in Fig. 4) is the axial wave-number index, defined in terms of the Fourier transform $F(k)$ of the luminance data, i.e.,

$$F(k)=\frac{1}{J}\sum_{j=1}^{J} f(j)\exp\left(\frac{-2\pi ikj}{J}\right),$$

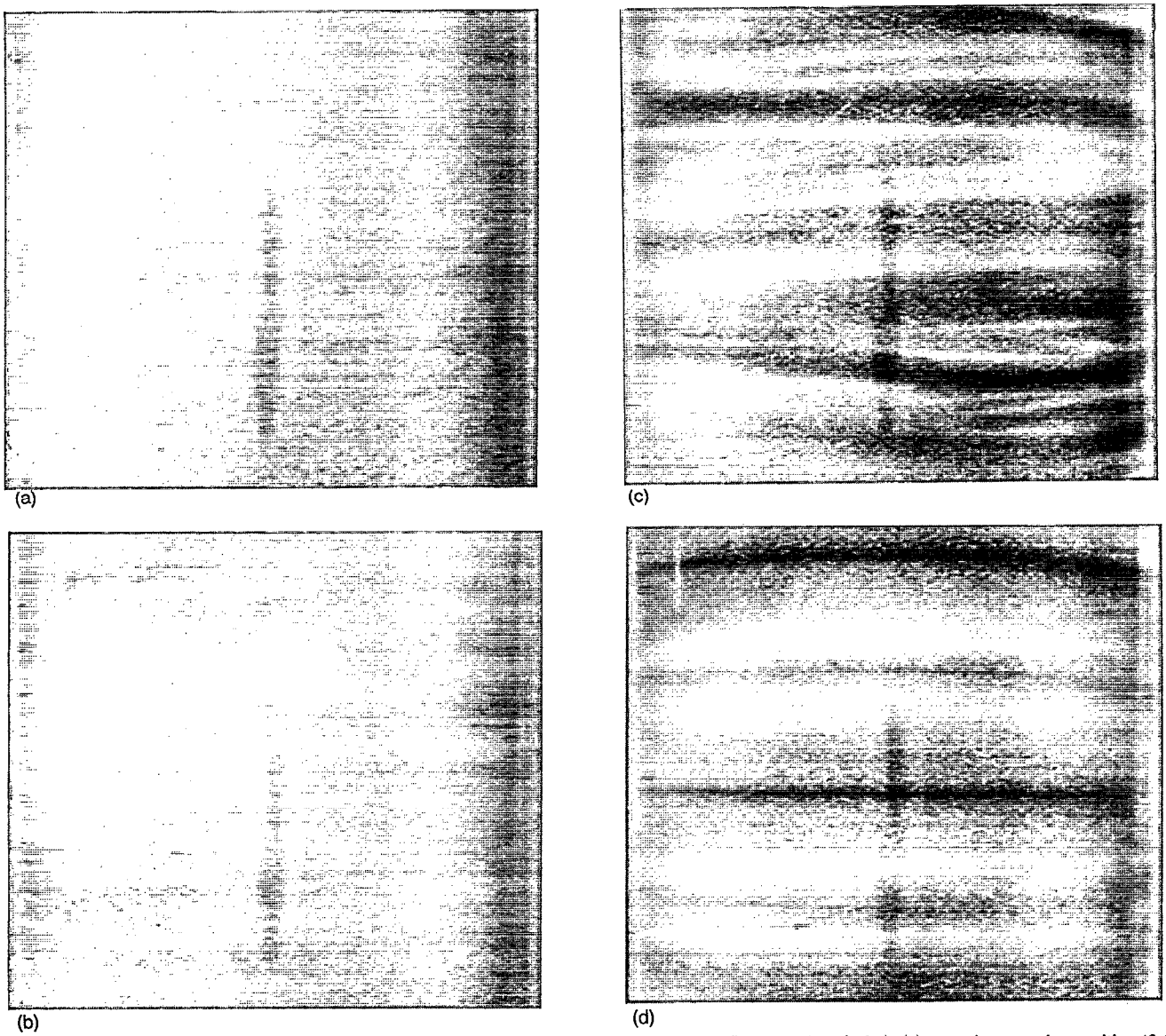

FIG. 2. (a)–(d) Instability sequence for Re=300: (a) unsteady swirl (0.47 s); (b) axisymmetric Görtler vortices (1.8 s); (c) nonaxisymmetric transition (2.6 s); (d) axisymmetric Taylor vortices (35 s).

where J is the number of data points in the axial direction. The *dimensional* axial wavelength λ_D is obtainable from $\lambda_D = l/k$, where l is the length of the luminance data line. Further details may be found in the thesis of Kirkconnell.[15]

TABLE I. Experimental results: t_0, onset time of initial, axisymmetric instability; t_t, onset time of nonaxisymmetric transition; Δt, onset time difference; λ, dominant axial wavelength of initial, axisymmetric instability; m, dominant azimuthal wave number at transition to nonaxisymmetric flow. All times are scaled by the gap-diffusion time; all lengths are scaled by the gap width. Differences between Δt shown in table and those computed from given t_0 and t_t values are due to round-off.

Re	t_0	t_t	$\Delta t = t_t - t_0$	λ	m
200	0.051	0.071	0.021	1.70	1
225	0.038	0.049	0.012	1.48	1
250	0.029	0.039	0.010	1.45	1
275	0.026	0.036	0.010	1.43	1
300	0.021	0.029	0.009	1.10	1

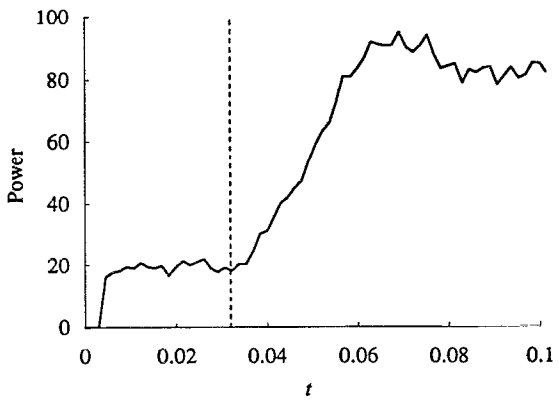

FIG. 3. Time evolution of the sum of the axial, non-DC spectral components ($k<16$) for Re=250 showing the predicted onset time of the initial instability. The amplitude equals zero for $t<0.004$ due to data conditioning.

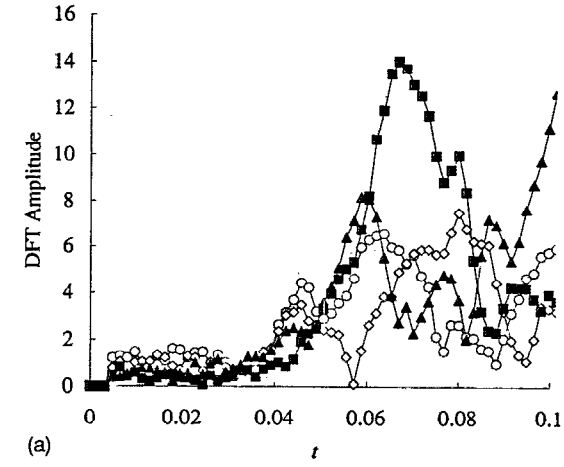

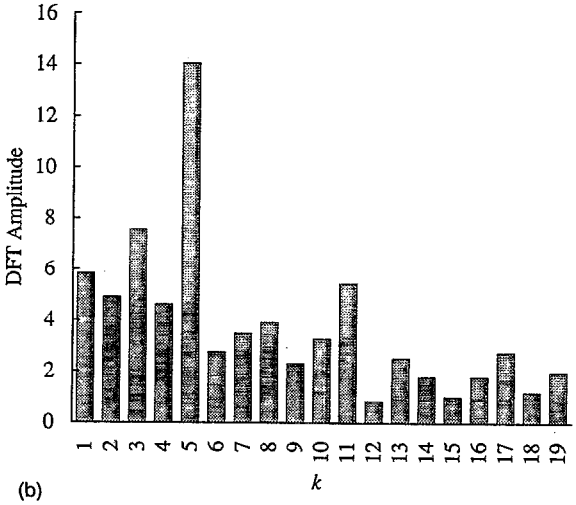

FIG. 4. (a) Spectral history of several distinct axial wave numbers for the same experiment depicted in Fig. 3: ○ $k=1$; ◇ $k=2$; ■ $k=5$; ▲ $k=6$. The interactions of the wave numbers complicate the prediction of the onset time; (b) spectrum corresponding to $t=0.065$.

The time at which the amplitude begins to increase rapidly is identified as the *onset time* of the initial, axisymmetric instability. The *critical wave number* is defined as the first wave number to exhibit such rapid growth in amplitude, and this information was obtained from the first type of graph, an example of which is shown in Fig. 4(a), which shows the DFT amplitude history of a few of the more powerful modes. In Fig. 4(b) is shown the complete spectrum corresponding to the time $t=0.065$, corresponding to the location of the maximum amplitude shown in Fig. 4(a). The same technique was applied to the azimuthal data to identify the onset and structure of nonaxisymmetric flow.

Since such graphical analyses are obviously subject to personal interpretation, a more quantitative method was sought. A statistical scheme similar to that used previously[3] was devised to determine the onset time and critical wave number by comparing the difference between a central-running average of the power (using N_1 data points) and a backward-running average (of the first N_2 data points) to a multiple (B) of the central-running standard deviation. Unfortunately, it was impossible to find a single set of constants

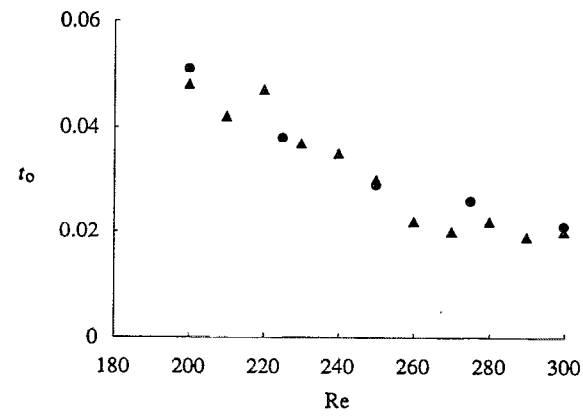

FIG. 5. Onset of the initial instability versus Reynolds number: ● present results; ▲ Kohuth and Neitzel[3].

N_1, N_2, and B which would yield an onset time of either instability consistent with visual observations for all experiments. Therefore, all of the onset-time results which are presented were obtained from a visual examination of either the video tape or the graphs of the power spectra.

Four quantities were desired for each experiment: (i) the onset time of the initial instability; (ii) the dominant axial wavelength at the onset of instability; (iii) the onset time of the transition to nonaxisymmetric behavior; and (iv) the dominant azimuthal wave number at the onset of the transition. All times have been scaled by the diffusion time d^2/ν and axial wavelengths are scaled by the gap width d. Five experiments were performed at each of the selected Reynolds numbers; all results presented are mean quantities resulting from these experiments.

1. The initial instability—Onset time and critical axial wavelength

The results reported for the onset time t_0 of the initial instability were determined primarily from the video tape. Since the appearance of the initial instability is spotty in nature, resulting from spontaneous nucleation of disturbances along the wall of the outer cylinder, the results obtained from the video tape were considered to be more representative of the true onset times because the entire field of view, rather than just a single vertical line, was available for observation. In the cases where the initial instability developed across the centerline of the cylinders, however, evidence of the instability appeared in the digitized power spectra of the axial structure at a slightly earlier time than it became visible to the naked eye. For such experiments, the result obtained from an examination of the power-spectra graphs is reported. The onset times obtained using a combination of the graphical technique described above and the video tape agree well with those of Kohuth and Neitzel,[3] as shown in Fig. 5.

Since the initial vortex pattern is very weak,[5] it is difficult to accurately measure the wavelengths of the Görtler vortices from the video-taped image as it appears on the monitor using image-processing software. Therefore, the results reported for the critical wavelengths were determined

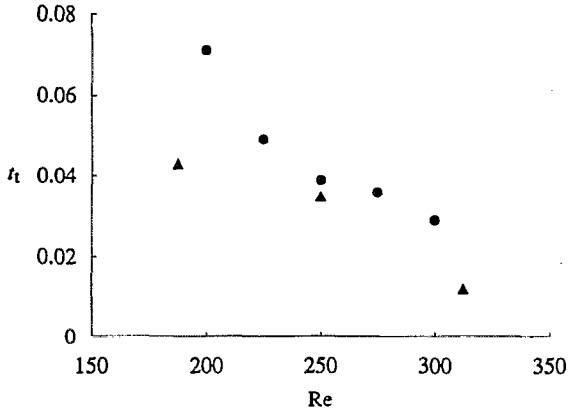

FIG. 6. Onset time of nonaxisymmetric flow versus Reynolds number: ● present results; ▲ Euteneur.[16]

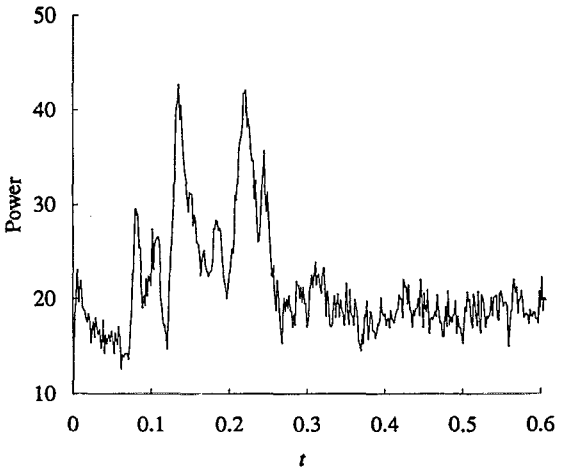

FIG. 7. Azimuthal power (sum of non-DC components) history for a case with Re=200 showing the transient nature of the nonaxisymmetric transition.

from analyses of the power content of individual wave numbers. As with the measurement of t_0, the critical wavelengths determined here compare favorably with those of Kohuth and Neitzel[3] and serve to validate the present data acquisition and reduction techniques.

2. Nonaxisymmetric flow—Onset time and critical azimuthal wave number

As with the axisymmetric results, the onset times t_t of the transition to nonaxisymmetric flow could be determined more accurately and consistently from the video tape than from the power spectra of the digitized luminance data since the entire field of view was available for examination. For a few of the experiments, the horizontal data-acquisition line happened to correspond with a region of the flow which did not exhibit any azimuthal structure until several seconds after the flow had clearly transitioned to the nonaxisymmetric regime. Typically, however, the transition times determined from an inspection of the video tape agree well with those determined from graphs of power spectra, regardless of whether a graph of individual wave numbers or the sum of the non-DC components was used. As with the analysis of the initial instability, the digitized data seems to be able to detect the development of the azimuthal structure at a slightly earlier time than can be detected visually if the data acquisition line crosses the region where the nonaxisymmetric disturbances first appears. For those experiments, the result determined from a graph of the power spectra was used. Otherwise, the transition time, as determined from a frame-by-frame analysis of the video tape, was reported.

The mean values for t_t, shown as a function of Re in Fig. 6, exhibit the expected decrease in onset time with increasing Reynolds number. Shown for comparison purposes are estimates for the same quantity observed by Euteneuer[16] (who referred to the transition as a "Knickstelle") for spin-down within a single cylinder. The difference $\Delta = t_t - t_0$ between the time of transition to nonaxisymmetric flow and the initial onset of instability, given in Table I, appears to be approaching a constant value for increasing Re. Although there is a decreasing trend in the mean values of Δt with increasing Re over the range investigated, the scatter does not permit a definitive statement to be made regarding the existence of a positive lower bound.

The critical azimuthal wave number m corresponding to Fourier mode $e^{im\theta}$ was determined to be $m=1$ for all of the experiments, whether from the graphed data or simply from a visual examination of the video tape [an $m=1$ tilting is apparent in the photograph of Fig. 2(c)]. The power spectra indicate a mildly significant contribution at the onset of the transition from the $m=2$ waves for two of the experiments at Re=225, but the presence of such modes could not be observed from the video-tape record. Therefore, the critical azimuthal wave number for all of these experiments is reported as $m=1$, but the possible contribution of higher wave numbers warrants further investigation. The numerical experiments on this problem to be discussed next also calculated $m=1$ as the dominant wave number at the transition to nonaxisymmetric flow, and Myers,[10] even with his poor resolution, obtained this same result.

The transient nature of the nonaxisymmetric flow regime, which is clearly visible in the photographs of Fig. 2, may also be seen by examining the long-time behavior of the power spectrum. Figure 7 shows the sum of the non-DC components of *azimuthal* power for a case at Re=200. Following an initial period of noise, during which the pure-swirl and Görtler modes are present, the azimuthal power increases for a time, then returns to the initial noise level after the establishment of axisymmetric, Taylor-vortex flow. The reason behind the *oscillation* of the power for $0.1<t<0.3$ is not known, but may be related to the fact that data are collected only along a single horizontal (azimuthal) line.

III. NUMERICAL EXPERIMENTS

A. Formulation

The governing equations for this problem are the incompressible Navier–Stokes and continuity equations. The gap width d is chosen as the length scale, the velocity is scaled by Ωd, the dynamic pressure $\rho(\Omega d)^2$ is used to scale the

pressure, and the time scale is chosen to be the diffusion time, d^2/ν. After scaling, the resulting equations are

$$\mathrm{Re}^{-1}\left(u_t+uu_r+\frac{v}{r}u_\theta+wu_z-\frac{v^2}{r^2}\right)=-p_r+\mathrm{Re}^{-1}\left(\nabla^2 u-\frac{u}{r^2}-\frac{2}{r^2}v_\theta\right), \tag{1a}$$

$$\mathrm{Re}^{-1}\left(v_t+uv_r+\frac{v}{r}v_\theta+wv_z+\frac{uv}{r^2}\right)=-\frac{1}{r}p_\theta+\mathrm{Re}^{-1}\left(\nabla^2 v-\frac{v}{r^2}+\frac{2}{r^2}u_\theta\right), \tag{1b}$$

$$\mathrm{Re}^{-1}w_t+uw_r+\frac{v}{r}w_\theta+ww_z=-p_z+\mathrm{Re}^{-1}\nabla^2 w, \tag{1c}$$

$$\frac{1}{r}(ru)_r+\frac{1}{r}v_\theta+w_z=0, \tag{1d}$$

where ∇^2 is given by

$$\nabla^2\equiv\frac{1}{r}\frac{\partial}{\partial r}\left(r\frac{\partial}{\partial r}\right)+\frac{1}{r^2}\frac{\partial^2}{\partial\theta^2}+\frac{\partial^2}{\partial z^2}, \tag{1e}$$

u, v, and w correspond to the velocity components in the radial, azimuthal, and axial directions, respectively, and

$$\mathrm{Re}=\frac{\Omega d^2}{\nu}, \tag{2}$$

is the *Reynolds number* defined previously to characterize the experiments. The initial condition is

$$u=0,\quad v=r,\quad w=0\quad \text{at } t=0, \tag{3}$$

and the boundary conditions to be applied are the kinematic and no-slip conditions at the inner and outer cylinders (4a),(4b) and an assumption of periodicity in the axial direction (4c):

$$u=w=0,\quad v=\frac{\eta}{1-\eta}\quad \text{at } r=\frac{\eta}{1+\eta}, \tag{4a}$$

$$u=v=w=0\quad \text{at } r=\frac{1}{1-\eta}, \tag{4b}$$

$$q(r,\theta,0)=q(r,\theta,\Gamma), \tag{4c}$$

where q represents any of the velocities or the pressure and Γ is the chosen length over which the flow is assumed periodic. Periodicity in the azimuthal direction with period 2π is also required. The condition (4c) requires some discussion. The domain of the flow to be computed is idealized to be infinite in axial extent and the flow is assumed to exhibit a periodic axial structure of dimensional period L allowing computations to be performed over a single periodic cell.[17] Such an assumption is consistent with the initial and final axisymmetric Görtler and Taylor-vortex states and assumed to hold for the regime of interest. The choice of the parameter Γ is a troublesome one, however, since a single value will not serve all possible steady or transient vortex patterns. More discussion of this point will follow.

B. NEKTON spectral-element code

The NEKTON code[18] uses the spectral-element method[19] to solve the time-dependent, incompressible Navier–Stokes and/or heat equations, as well as various subsets of these, in one, two, or three dimensions. The spectral-element method combines the exponential accuracy associated with spectral methods with the ease of implementation of finite-element methods. The main difference between the spectral-element and finite-element methods is that high-order spectral functions rather than simple, low-order polynomials are used to perform the elemental interpolation steps. This results in large systems of linear equations which, although sparse, provide spectral accuracy.

NEKTON uses Lagrangian interpolation on a Gauss–Lobotto–Legendre mesh. The overall temporal accuracy is specified as $O(\Delta t)$; spatial accuracy is given as $O[\Delta x^p \exp(-\alpha N)]$, where p is the problem dimensionality, N is the number of elements, and α is a constant. The first component of this error is due to the decomposition of the global domain into elements and the second is due to the spectral nature of the interpolating polynomials. Thus the order of the interpolating polynomials has a greater effect on reducing the error than the number of elements. The solution to the discretized linear equations is performed using a solver based on conjugate-gradient iteration for the implicit terms and matrix multiplication for the explicit terms.

A simulation is performed by specifying an elemental problem domain, along with initial and boundary conditions, through an interactive, graphical preprocessor. There are three basic tasks to be performed by the user. The first is the design of the computational domain, in terms of both the number of elements to be employed and the order of the interpolation polynomials which will be used. For a given machine, these two parameters are closely linked. The second is the selection of a method for formulating the discretized governing equations. Three options are provided: the split, stress, and nonstress options. The primary difference in these formulations is in accuracy, execution time, and applicability to certain problems. Finally, a time step must be specified, however, the code will modify this time step if necessary in order to ensure Courant–Friedrichs–Levy stability[20] of the convection terms. The code then solves the equations for either a specified final time or number of time steps.

The user also specifies the form of the desired output. This can be either a complete dump of field variables or the time history of the field variables at specific nodal locations. The latter are referred to as history points. While the user can specify the frequency of the field dumps, there is no way to limit the rate of output of history points. Analysis of the results of a simulation is accomplished by a post-processor, which allows the computed quantities to be displayed graphically.

In spite of its generality, there are some limitations to the code (Version 2.7, used for the calculations reported here, is described; the current version referenced in the bibliography is 2.85). First, three-dimensional calculations are performed in Cartesian coordinates only, meaning that a purely axisymmetric solution may be more difficult to attain. Second, the

selected order of the expansion polynomials must be the same in all coordinate directions. Therefore, the only way to increase accuracy in a particular direction to resolve sharp gradients is to add more elements. Third, there is no provision to allow the user to output field variables for a subdomain of the flow to an external file for additional processing, although possible in previous versions of the code.

C. Numerical procedures

The numerical procedures necessary to perform the fully three-dimensional Taylor–Couette problem can be divided into three main parts: domain design, computation of the solution, and data reduction. The majority of the calculations referred to here were performed on an IBM RISC/6000 (model 530) workstation located at the Georgia Institute of Technology. Preliminary computations[21] on a related problem indicated that, of the three formulations available in NEKTON, the split formulation provides accuracy equal to the other formulations with a substantial reduction in CPU time; hence, it is the formulation employed for the results presented here.

The design of the computational domain is perhaps the most important part of the preparation for the computation. In accomplishing this, there are two primary considerations, namely, the selection of the type of domain (and the associated geometric domain parameters) and its discretization into spectral elements, including selection of the order of the interpolating polynomials. A truncated, infinite domain with periodic end conditions was selected as the domain type for this problem, as already mentioned. Other types were examined, however, including a complete, finite domain with fixed boundary conditions at the ends to correspond to the conditions of the laboratory experiments and a finite, half-domain with a fixed boundary condition at the cylinder base and a symmetry boundary condition at the midplane. Unfortunately, memory limitations of the RISC/6000 machine would not allow adequate resolution with a domain other than the axially periodic one employed.

As mentioned earlier, a single aspect ratio will not allow the accurate representation of all possible flow states, due to the fact that smaller, initially appearing, Görtler vortices ultimately give way to larger, Taylor vortices. The aspect ratio which was decided upon for the present computations was selected with the final, steady Taylor-vortex state in mind. It is well known that Taylor-vortex flow consists of pairs of counter-rotating vortices, each vortex being approximately square in cross section. Thus, if the dimensional gap width between the cylinders is d, the height of the domain required for K pairs of vortices is approximately $2Kd$. To ensure that proper behavior at steady state is realized, the aspect ratio must be selected such that the Taylor vortices appear in pairs of equal and opposite strength. Numerical experimentation resulted in the selection of an aspect ratio for these computations of $\Gamma=2.0$. The radius ratio used was set to $\eta=0.5$ to allow comparison with the experiments.

The final consideration in the domain design is the selection of the discretization (in terms of spectral elements) and the order of the interpolation polynomials. Many different domains were examined. This part of the design process involves examining the trade-offs between the number of elements and the order of the interpolating polynomials. Numerical experiments on a simpler, related problem resulted in the selection of the mesh shown in Fig. 8; it has 160 elements and uses fifth-order interpolation polynomials. The numbers of nodes in the r, θ, and z directions are 21,32, and 17, respectively, giving a total *unique* node count of 11 424. Oscillations are observed in flow quantities at small times in the computation immediately following the impulsive stop, but these diminish rapidly, prior to the appearance of the initial Görtler instability.

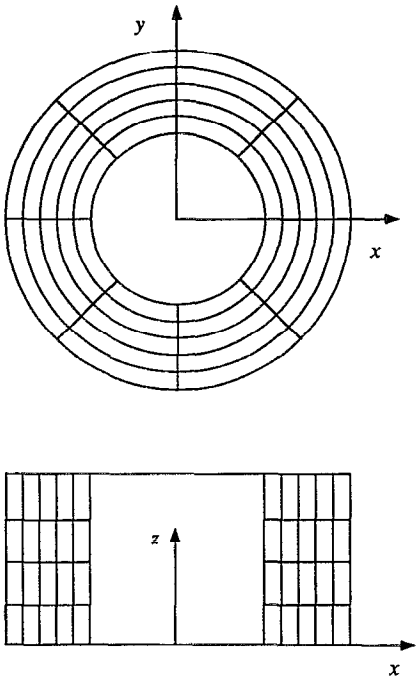

FIG. 8. Elemental mesh used in the solution of the unsteady CCF problem.

As discussed for the laboratory experiments, the power spectra determined by Fourier transforming flow quantities in the azimuthal direction were used to determine the onset times and azimuthal wave numbers for the nonaxisymmetric disturbances. The quantity selected for the computation of these power spectra was the z component of velocity, w, at 32 discrete, constant-radius, constant-height points around the cylinder. The points were chosen to be the nodes just inside the outer cylinder. This is to simulate, as well as possible, the results obtained from the laboratory experiments by the interpretation of flow-visualization data. The selected velocities were written to disk at every time step. The vertical velocity was chosen because of the necessity of solving the problem in Cartesian coordinates and the vertical velocity corresponds to the axial component in a more natural cylindrical coordinate system. Determination of the radial or azimuthal velocity components would entail additional computation and storage.

Although every time step is recorded, only 512 frames of data are actually used in the power-spectrum analysis, where a *frame* is defined as a complete set of vertical velocities for each of the 32 history points at a given time step. Since no mechanism exists in the code for limiting the rate of data

output, the excess points are discarded at the conclusion of each run. Each of the 512 records is Fourier transformed to obtain a power spectrum for each of the corresponding times. Since NEKTON only allows the recording of velocity histories at nodal locations, and since the Gauss–Lobotto–Legendre mesh nodes used in the program are not equally spaced in the azimuthal direction, a discrete Fourier transform (DFT) had to be used in place of a more efficient fast-Fourier transform (FFT).

Specific details of the statistical analysis can be found in Little.[21] It suffices to say that the onset of a particular wave number is determined to be the time at which a central running average of the amplitude spectra is greater than a constant multiple of a central-running standard deviation. The constant is chosen such that the onset times obtained agree visually with plots of the amplitude-spectra histories. The overall onset time t_t is then the minimum value of the onset times of all wave numbers, and the wave number m for which this occurs is deemed to be the critical one. Such an approach was unsuccessful with the laboratory data. We are concerned here only with the determination of the time at which the *nonaxisymmetric* transition appears. Storage of axially placed history data necessary to calculate spectra to locate the initial Görtler instability was prohibited, once again, by memory limitations.

D. NUMERICAL RESULTS

NEKTON was used to calculate the unsteady, three-dimensional impulsively initiated circular-Couette flow of interest for the case Re=300. This Reynolds number corresponds to one of the cases examined in the laboratory. In order to determine the time evolution of the flow structure, the 32 azimuthal history points just described were placed at $(r,z)=(1.965, 0.914)$, which is just inside the outer cylinder and slightly below the midplane of the computational domain.

Equally spaced temporal data were desired to simplify the statistical procedure used to determine the onset of times of transient, nonaxisymmetric instability. In order to obtain equally spaced time stepping, it was necessary to run the code twice. As mentioned earlier, NEKTON automatically adjusts the time step in order to satisfy the Courant–Friedrichs–Levy stability condition. For cases in which there are large variations in the flow velocities over the course of a run, this results in the usage by NEKTON of unequal time steps. This automatic time-step selection can be overridden, however, it is necessary that stability criteria be observed. Consequently for the first run, the code was allowed to chose the time steps. These were recorded and, after completion of the run, the minimum value, Δt_m, was noted. The code was then switched to a fixed-time-step mode and restarted, using a manually set time step equal to or smaller than Δt_m to ensure stability. For the case presented here, the time step was selected to be $\Delta t=8\times10^{-5}$. Another option, of course, would be to just interpolate the results from the runs with an automatically selected time step and then transform these data. This would yield spectra colored by the interpolation scheme used; since the RISC workstation was essentially a dedicated machine, it was decided to directly compute the results for equally spaced times.

Experimentation was also necessary in order to determine the time necessary to reach steady-state time. The results of Kohuth and Neitzel[3] and the present experiments were available to guide this aspect of the work. Knowledge of this time was necessary to ensure that the transition from axisymmetric (Görtler-vortex) flow to nonaxisymmetric flow and back to axisymmetric (Taylor-vortex) flow would be realized. The laboratory experiments revealed that a time of $t_s=0.8$ would be sufficient for all the pertinent flow regimes to be realized. This, coupled with the specified Δt, requires a total of 10 000 time steps. Certainly, for determination of the onset time of nonaxisymmetric modes alone, it is not necessary to compute the flow completely to steady state, but only to some time at which the nonaxisymmetric flow is evident. However, the more complete computation performed here lends credence to the ability of the code/model to at least qualitatively mirror the physics observed in the laboratory.

Figure 9 shows a time sequence of meridional-plane streamline histories for four different values of azimuthal angle θ. In Fig. 9(a), the streamlines indicate that the flow is still an axisymmetric swirl flow, i.e., no Görtler mode is yet visible, while in Fig. 9(b), these have clearly appeared, exhibiting only very weak azimuthal dependence. In Fig. 9(c), a definite loss of axial symmetry is clearly evident. Figure 9(d) shows that, at time $t=0.4$, the flow is still nonaxisymmetric, but the nonaxisymmetric effects are clearly decaying as compared to the previous plot. Finally, Fig. 9(e) shows the flow after it has essentially reached a steady state of Taylor-vortex flow. Thus, the computation appears to have represented, at least qualitatively, the transitions which are observed experimentally.

A graph of the power-spectra history for this computation is given in Fig. 10, in which only those azimuthal modes with sufficient power to be visible on the figure are shown. A comparison between Fig. 10 and its experimental counterpart (Fig. 7) shows a definite similarity, in that the transient nature of the nonaxisymmetric flow regime is clearly represented in both the computation and flow-visualization data. A casual inspection of these data reveals that the computed onset time appears to be around $t_t=0.04$ and that the onset wave number is $m=1$. The measured onset time for nonaxisymmetric flow for Re=300 was $t_t=0.029$. It is possible that the differences are due, in part, to the selection of the axial extent of the computational domain which coincides with the expected size of the final Taylor-vortex flow. Indeed, if the results of Fig. 9(b) are representative of the initial, Görtler-vortex mode, the presence of four pairs of vortices in the domain would correspond to an axial wavelength of $\lambda=0.5$, rather than the measured value of $\lambda=1.1$ (see Table I) for Re=300. In fact, a mode with the experimental axial wavelength is impossible to represent in this computational domain. Another possibility is that the vortices present in Fig. 9(b) are merely numerical in nature and not representative of the initial onset. Some evidence in support of this may be provided by the magnitude of the streamfunction, which is $O(10^{-3})$ for the case of Fig. 9(b), compared to $O(1)$ for the flow in Fig. 9(e) and the fact that the experimentally deter-

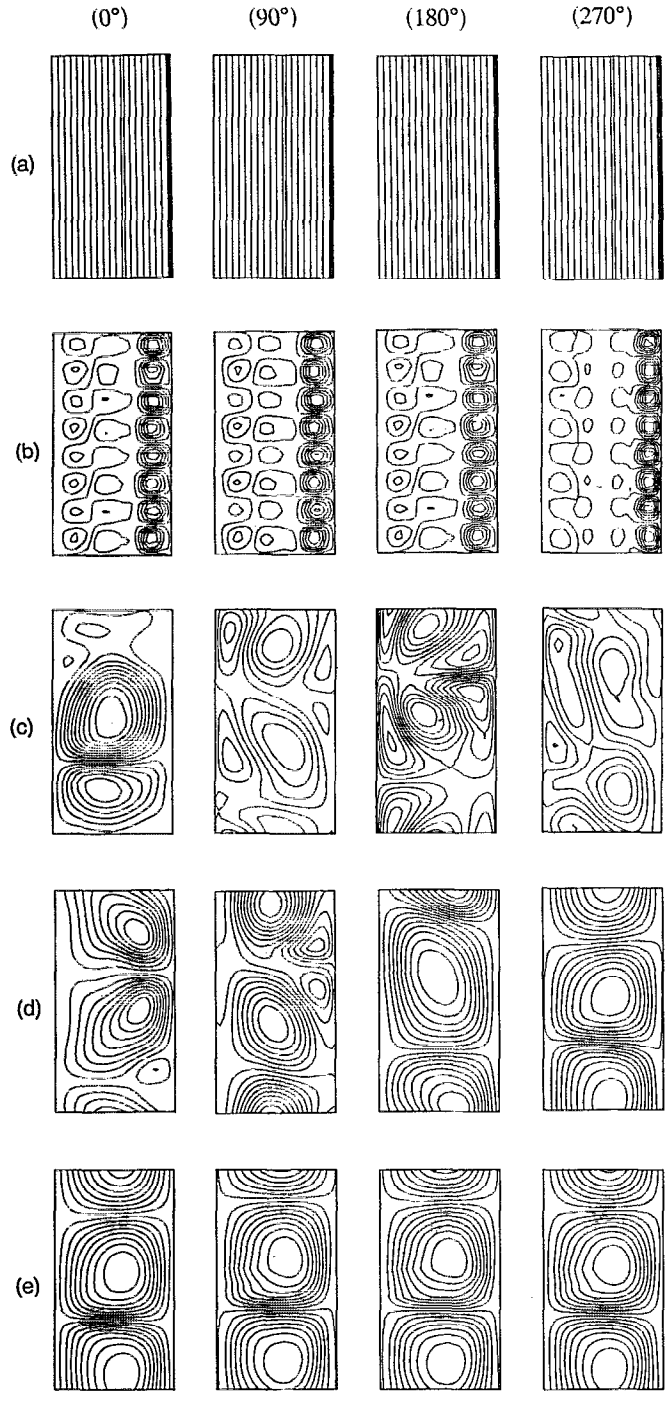

FIG. 9. Computed meridional streamlines at four azimuthal positions (0°, 90°, 180°, and 270°) at dimensionless times (a) 0.005; (b) 0.01; (c) 0.1; (d) 0.4; (e) 0.8. In all cases, the left and right boundaries correspond to the inner and outer cylinders, respectively.

mined onset time of $t_0=0.021$ is double the time of the computed state represented in Fig. 9(b).

An expanded plot of the spectral histories *prior* to time $t=0.04$ reveals contributions from $m=7$ and $m=15$ which are larger in amplitude than those of $m=1$, and a naïve statistical analysis would return the result that these correspond to the onset wave numbers. However, the magnitude of the power contained in these modes at these early times is two decades below that observed in Fig. 10, so that these contributions are more likely indicative of random noise than of a significant change in the flow. The statistical analysis for onset wave number $m=1$ revealed the onset time to be $t_t=0.0411$.

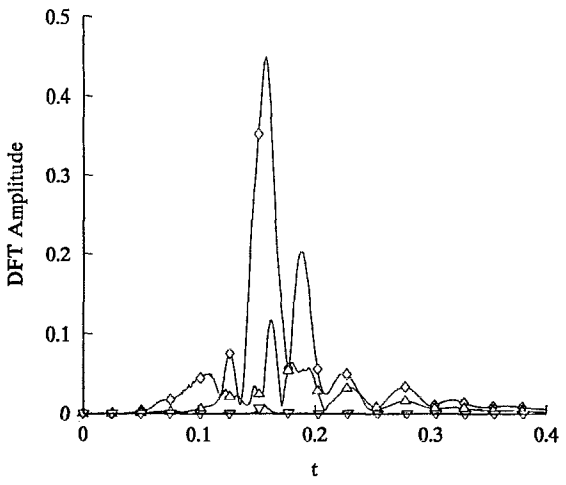

FIG. 10. Computed amplitude spectral histories for three azimuthal wave numbers: ◇, $m=1$; △, $m=2$; ▽, $m=7$.

IV. DISCUSSION

The primary goal of this investigation was to obtain quantitative results regarding the role of nonaxisymmetric modes in the selection of an axial pattern for this unsteady CCF. Both laboratory and numerical experiments indicate that the initially appearing, axisymmetric Görtler vortices lose stability to a nonaxisymmetric mode with an azimuthal wave number $m=1$ as the underlying swirl flow continues to decelerate. The ensuing adjustment of the vortices results, ultimately, in the establishment of a steady, axisymmetric Taylor-vortex state which persists indefinitely.

The laboratory experiments, performed with the use of flow visualization and digital photography, used a pair of horizontal and vertical lines along which to collect reflectance data, which was then Fourier transformed to examine the spectral character of observed spatial variations. In some instances, the horizontal line of data, from which the azimuthal variations were detected, coincided with a nodal line in the flow so that the true onset of nonaxisymmetry was not located by this technique, but rather, from an examination of the video tape. The collection of more on-line data during the course of the experiment would have significantly slowed the framing rate and also have required more extensive curvature corrections to be made prior to processing. The alternative is to flatten the image, either optically, prior to photographing the flow, or through software manipulation of the video-tape images. Neither of these was done for this set of experiments.

The numerical experiments utilized the code NEKTON, a spectral-element package capable of performing unsteady, three-dimensional computations. The results obtained appear to be valid in a qualitative sense, although they are not in complete quantitative agreement with those of the laboratory

experiments. The regimes observed experimentally[3] are all present in these computations. There is agreement between the azimuthal wave number measured at the onset of nonaxisymmetric flow and that computed here. The computed onset time for the Görtler-mode onset appears to be smaller than that observed in the laboratory while that computed for the nonaxisymmetric transition, however, is significantly higher. From Fig. 9(b), it would appear that the (unknown) value of the onset time for the initially appearing Görtler mode is, at most, $t_0=0.01$. The experimentally measured onset time of $t_0=0.021$ (Table I) indicates that the flow should still be pure swirl at this time. There are at least three possible reasons for this discrepancy. The first two, relating to the imposition of a fixed axial periodicity and the magnitude of the streamfunction, have already been discussed above. It would seem reasonable that a *smaller*-scale disturbance such as that computed here should have been visible in the laboratory experiments, if strong enough. The third reason could be related to the oscillations induced into the computations by the unrealistic, theoretical sudden stop. It is known that the instability results from an imbalance between the radial pressure-gradient force and the centrifugal force. Thus small inaccuracies in this profile could lead to premature onset times by serving as finite-amplitude disturbances.[17]

The problem of the axial extent of the computational domain for an unsteady problem of the type computed here is a troublesome one. One would like to compute the flow in a domain of limited axial extent from the standpoint of economy. Consequently, the computation reported here is performed under the assumption of axial periodicity with the length of the domain selected so that the final steady-state pattern is well represented. Numerical experiments by Chen, Neitzel, and Jankowski[17] have shown that, for a circular Couette flow with a ramped inner-cylinder speed, the proper steady state Taylor–Couette flow can be obtained for values of Γ in the range $1.9<\Gamma<2.1$. On the other hand, Liu and Chen[22] observe that aspect ratios less than 0.8λ where λ is the axial wavelength of one pair of Taylor vortices, will result in either no onset of instability or onset that is significantly delayed. Thus it is possible that the use of a truncated, infinite domain, regardless of Γ, will result in inaccuracies in the onset wavelength or onset time.

One remedy for this problem, of course, would be to perform the calculations in a complete, finite domain or at least a finite half-domain with a symmetric boundary condition at the midplane. Such calculations of unsteady axisymmetric swirl flows have been done by Neitzel and Davis[23] and Neitzel[9] with some degree of success. The inclusion of the third dimension, however, makes such an undertaking prohibitively resource expensive at the present time. The negative side of this, were it a practical solution, is that each computation is dependent upon the finite geometry selected. The ideal solution for the present problem would calculate the true infinite-cylinder problem, but such an effort must include allowing the computational domain to dynamically adapt to the changing flow structure.

ACKNOWLEDGMENTS

The authors would like to acknowledge Mr. S. Skinner for his assistance with electronics and Mr. J. P. Watson for assistance in the processing of computational data. We would also like to thank the referees for a very careful reading of the manuscript and several insightful comments. The work of one of the authors (GPN) was supported, in part, by the National Science Foundation under Grant No. CTS-8351490.

[1] J.-C. Chen and G. P. Neitzel, "Strong stability of impulsively initiated Couette flow for both axisymmetric and non-axisymmetric disturbances," J. Appl. Mech. **49**, 691 (1982).

[2] G. P. Neitzel, "Marginal stability of impulsively initiated Couette flow and spin decay," Phys. Fluids **25**, 226 (1982).

[3] K. R. Kohuth and G. P. Neitzel, "Experiments on the stability of an impulsively initiated circular Couette flow," Exp. Fluids **6**, 199 (1988).

[4] P. G. Drazin and W. H. Reid, *Hydrodynamic Stability* (Cambridge University Press, Cambridge, 1981).

[5] D. M. Mathis and G. P. Neitzel, "Experiments on impulsive spin-down to rest," Phys. Fluids **28**, 449 (1985).

[6] D. Coles, "Transition in circular Couette flow," J. Fluid Mech. **21**, 385 (1965).

[7] T. B. Benjamin and T. Mullin, "Notes on the multiplicity of flows in the Taylor experiment," J. Fluid Mech. **121**, 219 (1982).

[8] J. E. Burkhalter and E. L. Koschmieder, "Steady supercritical Taylor vortices after sudden starts," Phys. Fluids **17**, 1929 (1974).

[9] G. P. Neitzel, "Numerical computation of time-dependent Taylor-vortex flows in finite-length geometries," J. Fluid Mech. **141**, 51 (1984).

[10] W. R. Myers, "Experiments on non-axisymmetric disturbances in impulsively-initiated circular Couette flow," M. S. thesis, Arizona State University, 1990.

[11] R. D. Moser, P. Moin, and A. Leonard, "A spectral numerical method for the Navier–Stokes equations with applications to Taylor–Couette Flow," J. Comput. Phys. **52**, 524 (1983).

[12] P. S. Marcus, "Simulation of Taylor–Couette flow. Part 2. Numerical results for wavy-vortex flow with one travelling wave," J. Fluid Mech. **146**, 65 (1984).

[13] K. T. Coughlin and P. S. Marcus, "Modulated waves in Taylor–Couette flow. Part 2. Numerical simulation," J. Fluid Mech. **234**, 19 (1992).

[14] Ö. Savas, "On flow visualization using reflective flakes," J. Fluid Mech. **152**, 235 (1985).

[15] C. S. Kirkconnell, "Experiments on the stability characteristics of an unsteady circular Couette flow," M.S.M.E. thesis, Georgia Institute of Technology, 1992.

[16] G.-A. Euteneuer, "The development of longitudinal vortices in boundary layers growing with time along concave walls," Acta Mech. **13**, 215 (1972).

[17] J.-C. Chen, G. P. Neitzel, and D. F. Jankowski, "Numerical experiments on the stability of unsteady circular Couette flow with random forcing," Phys. Fluids **30**, 1250 (1987).

[18] NEKTON *Version 2.85 User's Guide* (Fluent, Lebanon, NH, 1992).

[19] A. T. Patera, "A spectral element method for fluid dynamics: laminar flow in a channel expansion," J. Comput. Phys. **54**, 468 (1984).

[20] P. J. Roache, *Computational Fluid Dynamics* (Hermosa, Albuquerque, 1976).

[21] L. J. Little, "Numerical experiments on non-axisymmetric disturbances in impulsively initiated circular Couette flow," M. S. thesis, Arizona State University, 1991.

[22] D. C. S. Liu and C. F. Chen, "Numerical experiments on time-dependent rotational Couette flow," J. Fluid Mech. **599**, 77 (1977).

[23] G. P. Neitzel and S. H. Davis, "Centrifugal instabilities during spin-down to rest in finite cylinders. Numerical experiments," J. Fluid Mech. **102**, 329 (1981).